NOTES AND CORRESPONDENCE

The Distribution of Rainfall over Oceans from Spaceborne Radars

WESLEY BERG AND TRISTAN L'ECUYER

Department of Atmospheric Science, Colorado State University, Fort Collins, Colorado

JOHN M. HAYNES

School of Mathematical Sciences, Monash University, Clayton, Queensland, Australia

(Manuscript received 19 June 2009, in final form 20 October 2009)

ABSTRACT

A combination of rainfall estimates from the 13.8-GHz Tropical Rainfall Measuring Mission (TRMM) precipitation radar (PR) and the 94-GHz *CloudSat* Cloud Profiling Radar (CPR) is used to assess the distribution of rainfall intensity over tropical and subtropical oceans. These two spaceborne radars provide highly complementary information: the PR provides the best information on the total rain volume because of its ability to estimate the intensity of all but the lightest rain rates while the CPR's higher sensitivity provides superior rainfall detection as well as estimates of drizzle and light rain. Over the TRMM region between 35°S and 35°N, rainfall frequency from the CPR is around 9%, approximately 2.5 times that detected by the PR, and the CPR estimates indicate a contribution by light rain that is undetected by the PR of around 10% of the total. Stratifying the results by total precipitable water (TPW) as a proxy for rainfall regime indicates dramatic differences over stratus-dominated subsidence regions, with nearly 20% of the total rain occurring as light rain. Over moist tropical regions, the CPR substantially underestimates rain from intense convective storms because of large attenuation and multiple-scattering effects while the PR misses very little of the total rain volume because of a lower relative contribution from light rain. Over low-TPW regions, however, inconsistencies between estimates from the PR and the CPR point to uncertainties in the algorithm assumptions that remain to be understood and addressed.

1. Introduction

Over ocean regions, global energy and water cycle studies rely almost exclusively on precipitation estimates from satellite remote sensing techniques. Although new sensor technologies combined with increased sampling from multiple infrared and passive microwave spaceborne sensors have led to the development of a number of new large-scale rainfall datasets, accurate information on the frequency and distribution of rainfall and how it changes between regions and over time is often limited (Petty 1995, 1997). Trenberth et al. (2003) argue that the characteristics of precipitation (i.e., the frequency and intensity) are just as vital as the amount. They point out that "[c]limate change is certainly very likely to locally change the intensity, frequency, duration, and amounts of precipitation," thus requiring "better documentation and processing of all aspects of precipitation." As an example, Karl and Knight (1998) found evidence of an approximately 10% increase in precipitation over the contiguous United States since 1910, noting that this increase was primarily due to an increase in the frequency and intensity of heavy- and extreme-precipitation events, with no systematic increase in the median rainfall amount.

The distribution of rainfall intensity, also referred to as the rainfall probability density function (PDF), is affected by several factors including the spatial resolution of the rainfall observations, the sensitivity of the instrument, and uncertainties in the observations/estimates. Global rainfall datasets rely on estimates from passive microwave sensors because of their relatively frequent sampling and superior instantaneous estimates in

Corresponding author address: Wesley Berg, Dept. of Atmospheric Science, Colorado State University, Fort Collins, CO 80523-1371.
E-mail: berg@atmos.colostate.edu

DOI: 10.1175/2009JAMC2330.1

comparison with visible/infrared techniques (Ebert et al. 1996), however, the resulting rainfall PDF is limited by the poor spatial resolution of the sensors (best case is ~25 km) and the inability to distinguish rainwater from cloud water. The 13.8-GHz precipitation radar (PR) on board the Tropical Rainfall Measuring Mission (TRMM; Kummerow et al. 1998) currently provides the most direct observations of rainfall intensity over the tropics and subtropics, although the sensitivity of the PR is limited to ~17 dBZ. This results in an underestimate of the contribution of light rain and/or small, isolated rain events that fill only a portion of the 5-km field of view (FOV), although the extent of this underestimate by PR and how it varies with regime is unclear. A study by Schumacher and Houze (2000) using ground-based S-band validation radar data over Kwajalein Atoll, Republic of the Marshall Islands, in the western Pacific Ocean determined that the PR only missed about 2.3% of the near-surface rain volume but missed 46% of the near-surface rain area. In contrast, an analysis of PR data by Short and Nakamura (2000) found evidence that the PR undersamples shallow clouds over regions dominated by marine stratocumulus/stratus, thus raising the question of whether rain missed by PR might be a more significant issue over areas not dominated by deep convection.

Although the precise amount of light rainfall missed by the PR is unknown, the launch of the 94-GHz *CloudSat* Cloud Profiling Radar (CPR) in April of 2006 (Stephens et al. 2008) and the subsequent development of a CPR retrieval algorithm for estimating light rain provide a unique opportunity to assess the PDF of rainfall over tropical and subtropical oceans by combining estimates from these two spaceborne radars. The *CloudSat* CPR has a minimum detectable signal of −30 dBZ, making it sensitive to the onset of rainfall and useful for estimating the intensity of drizzle and/or light rain, although the effects of attenuation and multiple scattering severely limit the CPR's ability to estimate rainfall in systems with moderate–heavy rain. Thus, these two radars are highly complementary, because the CPR provides better information on rain frequency and light-rain intensity while the PR provides estimates of rainfall intensity for a wide range of precipitating clouds that vary in intensity from just below 1 mm h^{-1} to the most intense cells that produce rain in excess of 100 mm h^{-1}. In addition, although a scarcity of in situ observations over oceans makes it difficult to ascertain the magnitude of errors and/or limitations of the individual retrievals, comparisons between retrievals based on different sensor technologies can provide valuable insights into many of these issues (Berg et al. 2006).

2. Data

The TRMM PR rainfall estimates used in this comparison are from version 6 of the operational 2A25 retrieval algorithm developed by Iguchi et al. (2000). These estimates are based primarily on backscattered radiation from raindrops that nominally increases with the sixth moment of the raindrop size distribution (DSD). As a result, the PR rain-rate estimates, like those of conventional ground-based radar systems, derive primarily from the largest raindrops in the sample volume that constrain an assumed DSD by fixing the number of particles in the large particle tail of the distribution. It is perhaps not surprising, then, that the dominant source of uncertainty in PR rainfall estimates is the shape of the assumed DSD. Although the assumed DSD may be adjusted in moderate–heavy rainfall when the PR experiences sufficient attenuation to provide a reliable estimate of the path-integrated attenuation (PIA), the attenuation of the PR signal is negligible for light rain. This means that deviations in the DSD from the assumed value can lead to significant errors in the resulting estimate of rainfall intensity for light–moderate rain rates. In addition, Kummerow et al. (1998) suggest that the minimum rain rate that the PR can detect is around 0.7 mm h^{-1}, but this value is dependent on both the DSD and the variability within the ~5-km FOV. As a result, the PR is not an ideal sensor for investigating the distribution of light or small-scale rainfall.

The *CloudSat* CPR rainfall estimates used in this study are from release 4 (R04) of the "2C-PRECIP-COLUMN" algorithm developed by Haynes et al. (2009). The CPR retrieval estimates rainfall intensity by exploiting the strong attenuation of *CloudSat*'s 94-GHz CPR associated with the presence of drizzle and light rain. The technique is based on the fact that in clear skies the backscatter from the ocean's surface is determined, to first order, by surface wind speed and SST. The PIA in a raining scene can, therefore, be estimated as the difference between the observed surface return and the equivalent clear-sky value based on wind speed and SST. Although the retrieval uses the PIA to estimate the rain rate, rainfall detection is based on the attenuation-corrected reflectivity in the lowest clutter-free bin. Because the reflectivity initially increases with the sixth moment of the raindrop size distribution, the presence of raindrops results in a dramatic increase in the reflectivity, making the CPR very sensitive to the onset of rain. It is important to note that, although it has a spatial resolution of approximately 1.5 km, unlike the PR the CPR is not a scanning radar, and therefore it provides a single vertical profile along the flight direction. On the other hand, the PR scans across an approximately 250-km

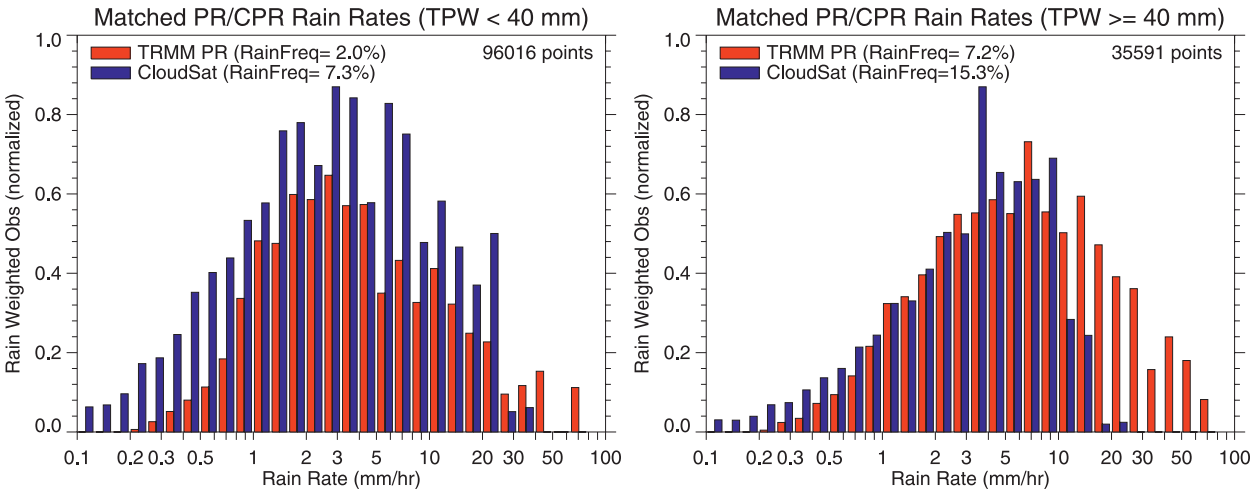

FIG. 1. The distribution of rain volume as a function of rainfall intensity over tropical and subtropical oceans based on collocated CPR and PR estimates for the period from June 2006 through February 2009. Shown are the rain-weighted occurrence of collocated rain rates corresponding to TPW (left) below and (right) above 40 mm. The CPR rainfall estimates have been averaged over the PR footprint to minimize the effect of differences in the FOV of the two sensors.

swath, although at a lower spatial resolution of approximately 5 km.

3. Results

Rain-rate histograms from *collocated* PR and CPR estimates are shown in Fig. 1 for the period from June 2006 through February 2009. Because of the low-inclination orbit of the TRMM spacecraft and the ocean-only coverage of the current CPR precipitation retrieval algorithm, the analysis is restricted to ocean regions between 35°S and 35°N. To account for differences in spatial resolution between the two sensors, the CPR estimates have been averaged within the ~5-km PR FOV. Crossovers between the polar-orbiting *CloudSat* and the tropical TRMM orbit within a specified 5-min time window occur approximately 2 times per day on average. Although the nadir-only view of the CPR limits the number of samples available for direct comparison, a total of 131 607 collocated pixels were available over the nearly 3-yr period analyzed, with ~10% identified by the CPR retrieval as raining.

The results in Figs. 1a/1b have been stratified based on corresponding total precipitable water (TPW) estimates above/below 40 mm from the Remote Sensing Systems Co. (Wentz and Spencer 1998). TPW is used here as a proxy for rainfall regime, because it was previously demonstrated by Berg et al. (2006) to be highly correlated with biases between rainfall estimates from the TRMM PR and TRMM Microwave Imager (TMI), which is due in large part to the relationship between TPW and the vertical structure of rain systems over the TRMM ocean coverage domain. This is demonstrated in Fig. 2 by two-dimensional histograms of the PR echo-top height, indicating the top of the rain column, and Visible and Infrared Scanner (VIRS) channel-4 infrared brightness temperatures, indicative of cloud top, for various ranges of TPW. There are clear and dramatic changes in the types of rain clouds for different amounts of TPW, with shallow warm systems dominating in low-TPW environments and deeper convective systems that dominate the high-TPW environments found in the tropics.

The results shown in Fig. 1b for TPW values above 40 mm indicate excellent agreement between the CPR and the PR rainfall estimates over the range from around 1 to 3 mm h^{-1}. As expected, the PR distribution starts to fall off below 1 mm h^{-1} and the CPR estimates drop off above 10 mm h^{-1}. Because of the limited number of samples, it is not possible to ascertain whether differences in the range from 3 to 10 mm h^{-1} are significant. The results shown in Fig. 1a for TPW values below 40 mm indicate much poorer agreement between the two retrievals, with the CPR detecting more rain for a wide range of intensity. In the range from 1 to 2 mm h^{-1} the CPR produces nearly 35% more rain for these low-TPW matches, with the greatest disparity evident for the lowest TPW values (not shown). This result suggests that retrieval errors may be a significant issue over these colder, drier regions. Potential factors contributing to this discrepancy include systematic errors in DSD, uncertainty in the partitioning of cloud water versus rainwater, the shape of the vertical profile including the impact of evaporation at lower levels, inhomogeneity in the FOV, and errors in the assumed freezing height.

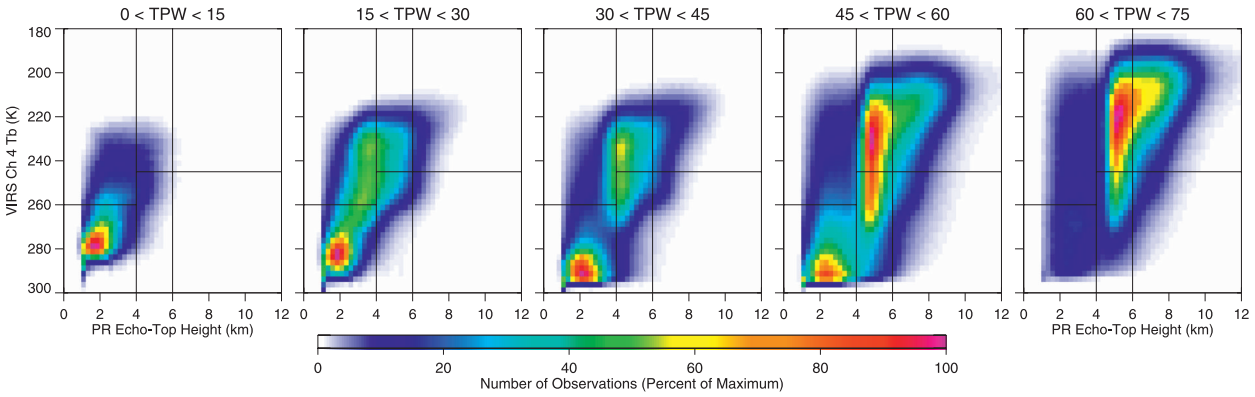

FIG. 2. Two-dimensional histograms of the frequency of occurrence of clouds as a function of the PR echo-top height and the VIRS channel-4 infrared brightness temperature as developed by Masunaga et al. (2005). Each panel corresponds to a separate TPW regime as indicated by the labels.

Note that, because of the orbit geometry, a majority of the orbit intersections occur at latitudes between 30° and 35°N/S and therefore predominately at low values of TPW.

Because of the limited number of collocated PR and CPR estimates available, rain-rate histograms from the entire unmatched (i.e., not collocated) PR and CPR populations are shown in Fig. 3 for the period from June 2006 through February 2009. As in Fig. 1, the CPR rainfall estimates are averaged over five pixels to account for differences in the ~1.5- versus ~5-km spatial resolution of the CPR and the PR, respectively. The PR estimates are further limited to near-nadir views to minimize surface-clutter effects. Because the two sensors have very different sampling populations from which these histograms are produced, three rain-rate zones are identified to facilitate their comparison. Zone 1 covers light rain rates up to 1 mm h^{-1} where the CPR has much better sensitivity than PR. Zone 3 covers moderate to heavy rain rates where multiple scattering and saturation of the attenuation signal at 94 GHz can limit the ability of the CPR to obtain quantitative rain estimates—in particular, for intense and/or deep systems in the tropics. Zone 2 covers a narrow ''transition zone'' in which both sensors have good sensitivity and can provide reasonable rain-rate estimates (Haynes et al. 2009; Iguchi et al. 2000), although as demonstrated in Fig. 1a algorithm errors may still exist. Given this overlap in instrument sensitivity, the rain PDFs in Fig. 3 have been scaled so that the total rainfall contribution within zone 2 is the same for both sensors. This was done to facilitate comparisons by effectively normalizing both PDFs to an equivalent sample size. This means that the full PR and CPR distributions were scaled such that the area under the solid red and blue curves in Fig. 3 between 1 and 2 mm h^{-1} is identical, which in this case is 12% of the total rain as indicated in the embedded ''rainfall volume'' table. This provides a simple way to compare these two disparate populations even though it does not fully account for differences in resolution and/or errors due to algorithm assumptions. The resulting best estimate of the full rain-rate distribution over tropical and subtropical oceans is provided by the CPR below 1 mm h^{-1} (indicated by the thick solid blue line) and the PR above 2 mm h^{-1} (indicated by the thick solid red line), with a transition between 1 and 2 mm h^{-1}.

The results in Fig. 3 are consistent with the results from the collocated data in Fig. 1, indicating significantly more light rain from the CPR, because of its greater sensitivity, and substantially more intense rain from the PR, because of the inability of the CPR to penetrate intense and/or deep rain systems as well as because of the effects of multiple scattering (Haynes et al. 2009). The rainfall-volume table embedded in Fig. 3 shows the relative rainfall contribution from each of the three rain-rate zones for the combined CPR + PR distribution as well as for the individual sensors. Given that the PR misses light rain and the CPR misses heavy rain, the total rain has been defined as the contribution from the spatially averaged CPR estimates in zone 1 (solid blue line), plus the contribution from zone 2, which is, by definition, the same from both sensors, plus the contribution from the PR in zone 3 (solid red line). As a result, only the combined CPR + PR histogram adds up to 100% of the rain volume. For rain rates below 1 mm h^{-1} (zone 1), the CPR indicates 2 times the contribution of the PR, with 17% versus 8%, which translates to around 10% of the total rain missed by PR. Conversely, in zone 3, PR indicates a bit less than 2 times the contribution from moderate–heavy rain of the CPR, suggesting that the CPR misses around 30% of the total rain.

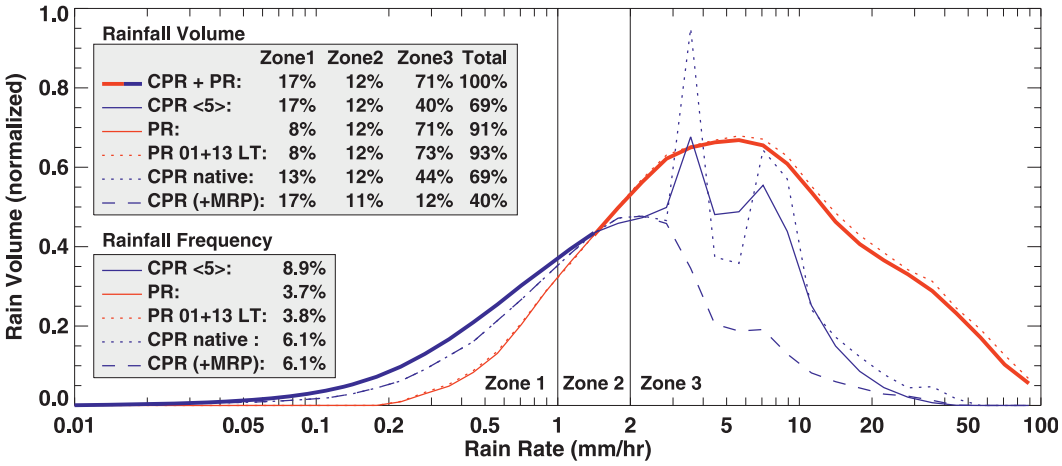

FIG. 3. The distribution of the total rain volume from the CPR and PR as a function of rainfall intensity over tropical and subtropical oceans (35°S–35°N) for the period from June 2006 through February 2009. The range of values within each bin is based on the logarithm of the rain rates. The number of observations within each bin is multiplied by the rain rate to indicate the relative contribution of both the lowest and highest rain rates in the distribution to the total rainfall. The complete PR distribution (solid red line) is shown along with the PR estimates subsampled at the local *CloudSat* observing times (dotted red line). The CPR estimates averaged over five adjacent pixels (solid blue line) are shown along with the native resolution CRP estimates (dotted blue line) and with the estimates exceeding the MRP removed (dashed blue line).

4. Discussion

As mentioned previously, the shape of the rain PDF is affected by several factors, including the spatial resolution of the rainfall observations, the sensitivity of the instrument, and uncertainties in the observations/estimates. Differences in the shape of the PR and CPR rain-rate histograms in zone 2 suggest that, even over this narrow range of rain rates, differences in sampling and/or algorithm errors may influence the statistics from each sensor. The effect of spatial resolution on the histograms is indicated by the differences between the solid and dotted blue lines in Fig. 3, which show results for the ''native'' 1.4 km × 1.7 km CPR FOV versus five adjacent CPR pixels averaged together. Although the resolution of the five averaged nadir CPR pixels is still somewhat less than that of the ~5-km FOV of the PR, the differences between the solid and dotted blue lines in Fig. 3 provide a crude estimate of the expected resolution differences on the resulting histogram. Note that in zone 1 the dotted and dashed (described below) blue lines overlap, creating a dashed/dotted line. Adjusting the CPR results to match the resolution of the PR is more complicated than simply averaging a specified number of pixels together, because the effect of averaging depends on the homogeneity of rain across the PR FOV. As Fig. 3 indicates, however, the effects of averaging are generally small when compared with the PR–CPR differences themselves.

Another factor to consider is the effect of the diurnal cycle on the distributions. Because of its sun-synchronous orbit, *CloudSat* overflies a given point on the earth at the same local times each day, roughly 0130/1330, whereas TRMM samples the entire diurnal cycle. The dotted red line shown in Fig. 3 indicates the impact of subsampling the PR observations to include only those observations between 0100 and 0200 and between 1300 and 1400 local time, which roughly corresponds to the local times as sampled by the CPR. As the results in Fig. 3 indicate, differences due to the time of day of the observations are minimal because of the small magnitude of the diurnal cycle over oceans.

The effects of algorithm biases on the PR and the CPR retrievals also need to be considered. For heavy rain cells where the intensity of the rain cannot be accurately estimated, the CPR retrieval flags indicate rain rates exceeding a calculated maximum retrievable precipitation rate (MRP). While the MRP can exceed 10 mm h^{-1} for shallow clouds at higher latitudes, for deep systems in the tropics it is substantially less (Haynes et al. 2009). These values are stored as negative rain rates in the CPR datasets and serve primarily to indicate the presence of rainfall. The effect of removing these values is indicated by the dashed blue line shown in Fig. 3. As expected this has no impact on the light rain rates in zone 1, but it dramatically reduces the estimated rainfall in zone 3 for rain rates greater than 3 mm h^{-1}. As the solid and dotted blue lines that include these values indicate, rainfall estimates exceeding the MRP tend to produce nonphysical spikes around 3.5 and 7.5 mm h^{-1} in the intensity spectrum. Since they merely represent

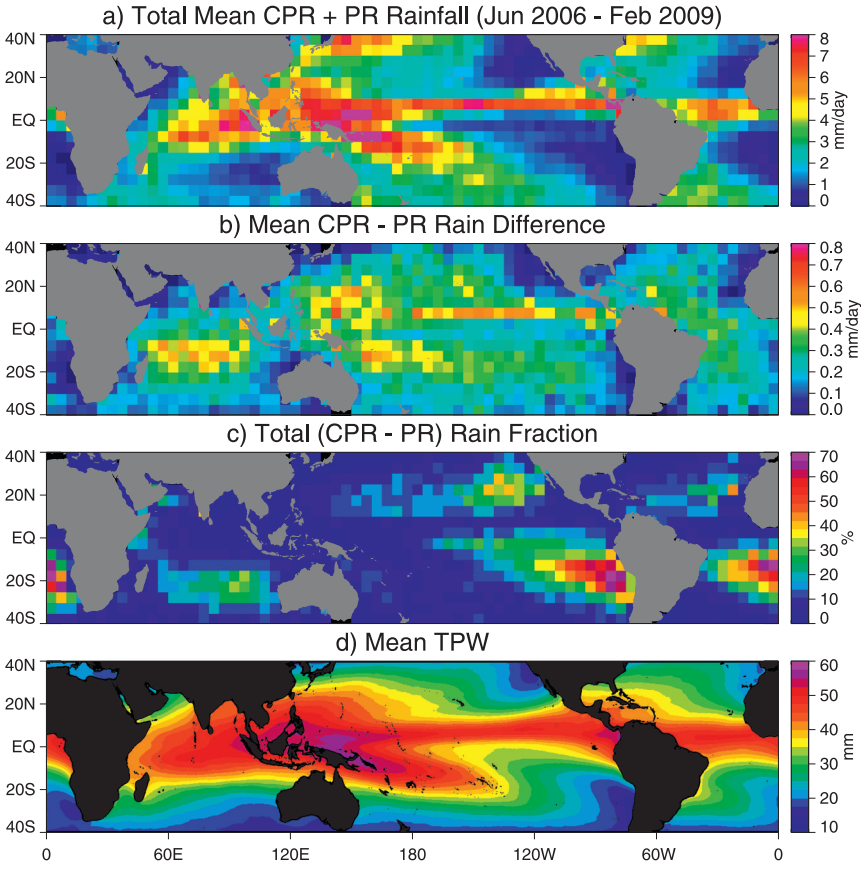

FIG. 4. (a) The total mean rainfall determined from the combination of PR and CPR estimates for the period from June 2006 through February 2009, the (b) total and (c) fractional contribution from the CPR missed by the PR, and (d) the mean TPW for the corresponding period.

the minimum rain rate for a given profile the actual rain rate is likely higher, but cannot be uniquely measured with the CPR (Haynes et al. 2009). These values have been included in this analysis because the CPR observations contain information regarding heavy rainfall that is important to consider when comparing with estimates from other sensors such as the PR, although it is necessary to realize that the associated uncertainties tend to be large. It should also be noted that when the CPR estimates are averaged for comparison with the PR the values exceeding the MRP can impact the distribution of the lighter averaged rain rates, although the effect is small and limited to deep systems in the tropics.

Differences in the frequency of occurrence of rainfall for the various cases discussed above are given in the embedded ''rainfall frequency'' table in Fig. 3. Over the tropical and subtropical ocean region analyzed, almost 9% of the spatially averaged CPR estimates are raining, as compared with only 3.7% for the PR. Differences in spatial resolution also have a significant impact on the rainfall fraction with the frequency of rainfall occurrence dropping to 6.1% at the native CPR resolution.

The approach used to normalize the CPR and PR estimates in Fig. 3 has also been applied to individual $5° \times 5°$ grid boxes to create a map showing the geographical distribution of light rain missed by the PR. The resulting difference in the rain volume between the PR and CPR estimates within zone 1 (i.e., RR < 1 mm h^{-1}) is shown in Fig. 4b. As compared with the total mean rainfall from the combined PR and CPR estimates shown in Fig. 4a, it is apparent that the largest overall contribution from light rain (shown in Fig. 4b) occurs over areas with the highest total rain. It is also evident from this figure that the contribution from light rain correlates well with the map of TPW shown in Fig. 4d. Conversely, Fig. 4c shows the contribution of light rain missed by the PR as a fraction of the total rainfall, which indicates that the highest fractional contribution occurs

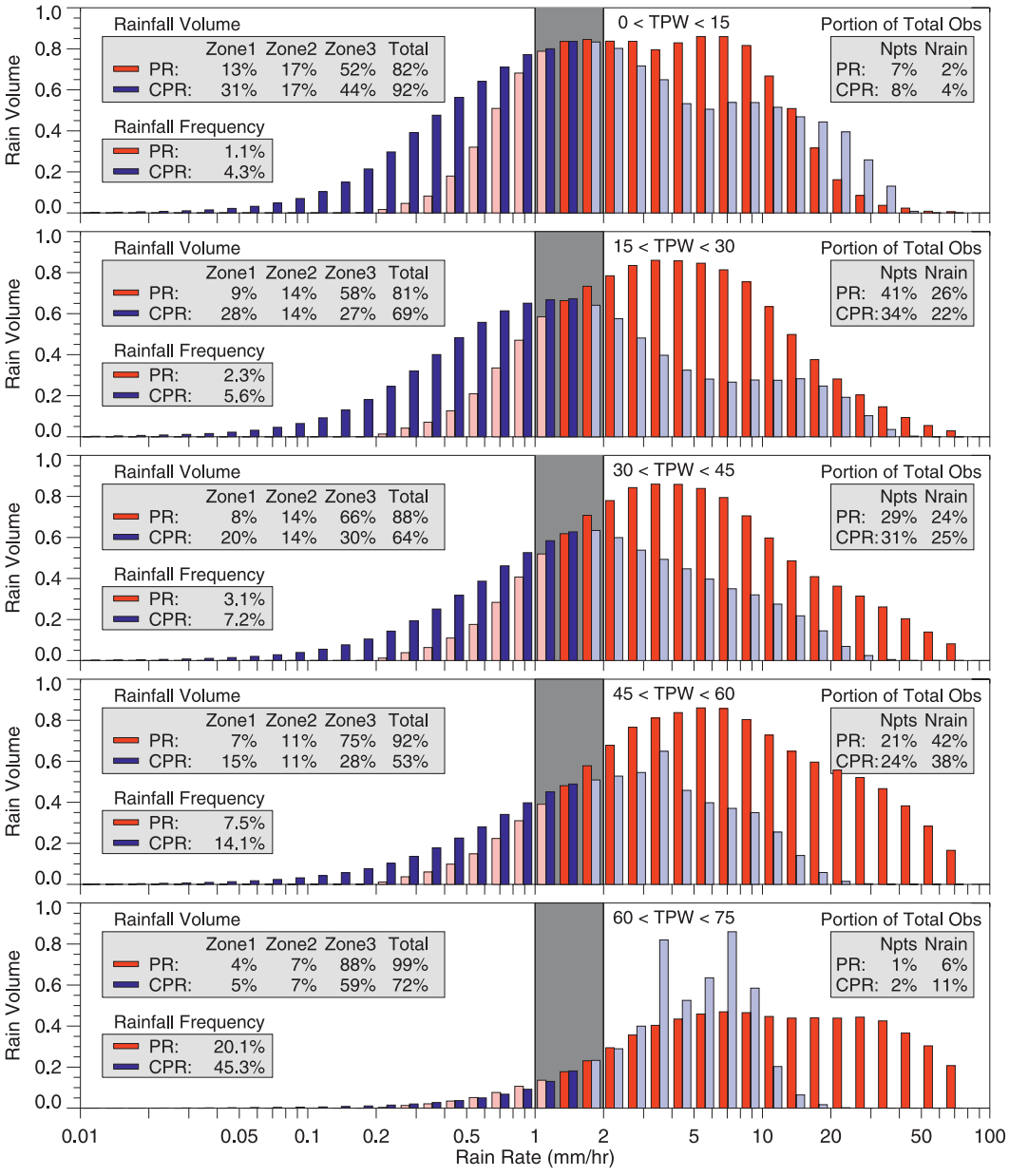

FIG. 5. The distribution of rain volume as a function of rain rate over tropical and subtropical oceans from the PR and CPR as a function of TPW, ranging from (top) 0–15 mm to (bottom) 60–75 mm. For each TPW range, both the rainfall frequency and the contribution to the total rainfall volume within each rain-rate zone are provided in the embedded tables. Zone 1 is below 1 mm h^{-1}, zone 3 is above 2 mm h^{-1}, and zone 2 (dark gray shading) is between 1 and 2 mm h^{-1}. The numbers on the rhs of the plot indicate the contribution to the total histogram shown in Fig. 1 within the given TPW range. The combined PR/CPR histogram is indicated by the bright blue and red bars while the light red and blue bars indicate the range over which the PR/CPR underestimate because of a lack of sensitivity to light/heavy rain, respectively.

over the stratus-dominated subsidence regions off the west coast of South America and Africa.

The rain-rate histograms shown in Fig. 3 have been further stratified by TPW in Fig. 5. The normalization of the histograms done in Fig. 3 by equalizing the rainfall contribution from zone 2 was performed separately for each TPW range shown in Fig. 5. The contribution of light rain below the PR detection threshold is largest over the low-TPW regimes in Fig. 5a (0–15 mm) and Fig. 5b (15–30 mm), with almost 20% of the rain volume

and three-quarters of the rain frequency missed by the PR. As shown in Fig. 1a, this is also the TPW range with the largest discrepancies between the two retrievals. It is important to note, however, that the lowest and highest TPW ranges shown in Fig. 5 are not well populated, with 7%–8% of the observations in the lowest TPW range and only 1%–2% of the observations in the highest TPW range. Over the moist regions of the deep tropics, intense convective rain that can only be retrieved by the PR dominates the rainfall distribution. When TPW exceeds 45 mm, for example, the CPR rain-rate distribution not only misses a substantial fraction of the rain volume, but also exhibits artifacts due to rain rates exceeding the MRP. The lack of light rain in the highest TPW category, on the other hand, results in the PR missing less than one-half of the rain fraction and only 1% or so of the rain volume, consistent with the results of Schumacher and Houze (2000) over Kwajalein Atoll.

5. Summary

The combination of rainfall estimates from the *CloudSat* CPR and the TRMM PR provides a powerful tool for investigating the distribution of rainfall over tropical and subtropical oceans. Both sensors have limitations, but they provide highly complementary information. The PR provides the best information on the total rain volume because of its ability to estimate the intensity of all but the lightest rain rates while the CPR's higher sensitivity provides superior rainfall detection and is better for estimating the intensity of drizzle and light rain. The amount of light rain missed by the PR is highest over the convergence zones, but it accounts for a far larger fraction of the total rainfall over the subsidence zones. Using TPW as a proxy for meteorological regime indicates large changes in the distribution of rainfall between the dry subsidence regions and areas of moisture convergence. Light rain below the PR detection threshold provides a significant contribution to the total rainfall in the low-TPW regime, whereas the CPR is unable to retrieve a majority of the intense rain in the tropics. Overall, results from the CPR indicate that PR misses around 10% of the rain volume across the TRMM ocean region, but this varies from only 1% in the moist regions of the deep tropics to nearly 20% over drier extratropical regions. As expected, the PR misses a substantially larger fraction of rain occurrence, with the CPR detecting rainfall almost 2.5 times as frequently as the PR. The limitations of the CPR retrieval with respect to intense rainfall are also clearly evident, missing around 30% of the total rainfall over the TRMM ocean region and as much as 50% in areas of the deep tropics.

Inconsistencies between estimates from the PR and the CPR in the range from 1 to 2 mm h^{-1}, where both retrievals are expected to provide reasonable estimates, point to uncertainties in the algorithm assumptions that still need to be understood and addressed. This appears to be a particularly important issue in low-TPW regions and may result from a number of factors. For the PR, potential concerns include the assumed DSD and inhomogeneity within the FOV; for the CPR, the partitioning between cloud and rainwater and variations in the vertical structure of the rain profile, including the effects of evaporation at low levels, may lead to biases in the retrieved rain rates. Although these issues require further study, as Berg et al. (2006) showed with their comparisons of rainfall estimates from the TRMM PR and TMI, the results presented here demonstrate the value of combining the complementary information provided by the PR and the CPR rainfall estimates for gaining insights into the microphysical characteristics of precipitating systems.

Acknowledgments. Funding for this work was provided by NASA Grant NNX07AD81G. The TPW data used in this project were produced by Remote Sensing Systems and sponsored by the NASA Earth Science MEaSUREs DISCOVER Project.

REFERENCES

Berg, W., T. L'Ecuyer, and C. Kummerow, 2006: Rainfall climate regimes: The relationship of regional TRMM rainfall biases to the environment. *J. Appl. Meteor. Climatol.,* **45,** 434–454.

Ebert, E., M. J. Manton, P. A. Arkin, R. J. Allam, C. E. Holpin, and A. Gruber, 1996: Results from the GPCP Algorithm Intercomparison Programme. *Bull. Amer. Meteor. Soc.,* **77,** 2875–2887.

Haynes, J. M., T. S. L'Ecuyer, G. L. Stephens, S. D. Miller, C. Mitrescu, N. B. Wood, and S. Tanelli, 2009: Rainfall retrieval over the ocean with spaceborne W-band radar. *J. Geophys. Res.,* **114,** D00A22, doi:10.1029/2008JD009973.

Iguchi, T., T. Kozu, R. Meneghini, J. Awaka, and K. Okamoto, 2000: Rain-profiling algorithm for the TRMM precipitation radar. *J. Appl. Meteor.,* **39,** 2038–2052.

Karl, T. R., and R. W. Knight, 1998: Secular trends of precipitation amount, frequency, and intensity in the United States. *Bull. Amer. Meteor. Soc.,* **79,** 231–241.

Kummerow, C., W. Barnes, T. Kozu, J. Shiue, and J. Simpson, 1998: The Tropical Rainfall Measuring Mission (TRMM) sensor package. *J. Atmos. Oceanic Technol.,* **15,** 809–817.

Masunaga, H., T. S. L'Ecuyer, and C. D. Kummerow, 2005: Variability in the characteristics of precipitation systems in the tropical Pacific. Part I: Spatial structure. *J. Climate,* **18,** 823–840.

Petty, G. W., 1995: Frequencies and characteristics of global oceanic precipitation from shipboard present weather reports. *Bull. Amer. Meteor. Soc.,* **76,** 1593–1616.

——, 1997: An intercomparison of oceanic precipitation frequencies from 10 special sensor microwave/imager rain rate algorithms

and shipboard present weather reports. *J. Geophys. Res.,* **102,** 1757–1777.

Schumacher, C., and R. A. Houze, 2000: Comparison of radar data from the TRMM satellite and Kwajalein oceanic validation site. *J. Appl. Meteor.,* **39,** 2151–2164.

Short, D. A., and K. Nakamura, 2000: TRMM radar observations of shallow precipitation over the tropical oceans. *J. Climate,* **13,** 4107–4124.

Stephens, G. L., and Coauthors, 2008: *CloudSat* mission: Performance and early science after the first year of operation. *J. Geophys. Res.,* **113,** D00A18, doi:10.1029/2008JD009982.

Trenberth, K. E., A. Dai, R. M. Rasmussen, and D. B. Parsons, 2003: The changing character of precipitation. *Bull. Amer. Meteor. Soc.,* **84,** 1205–1217.

Wentz, F. J., and R. W. Spencer, 1998: SSM/I retrievals within a unified all-weather ocean algorithm. *J. Atmos. Sci.,* **55,** 1613–1627.